

Combinatorial screening of 3D biomaterial properties that promote myofibrogenesis for mesenchymal stromal cell-based heart valve tissue engineering

Jenna Usprech, David A. Romero, Cristina H. Amon
and Craig A. Simmons

Version Post-print/Accepted Manuscript

Citation (published version) Usprech, J., Romero, D. A., Amon, C. H., & Simmons, C. A. (2017). Combinatorial screening of 3D biomaterial properties that promote myofibrogenesis for mesenchymal stromal cell-based heart valve tissue engineering. *Acta biomaterialia*, 58, 34-43.

DOI <https://doi.org/10.1016/j.actbio.2017.05.044>

Copyright/License This work is licensed under the Creative Commons Attribution-NonCommercial-NoDerivatives 4.0 International License. To view a copy of this license, visit [Creative Commons BY NC ND 4.0 License](https://creativecommons.org/licenses/by-nc-nd/4.0/).

How to cite TSpace items

Always cite the published version, so the author(s) will receive recognition through services that track citation counts, e.g. Scopus. If you need to cite the page number of the **author manuscript from TSpace** because you cannot access the published version, then cite the TSpace version **in addition to** the published version using the permanent URI (handle) found on the record page.

This article was made openly accessible by U of T Faculty.
Please [tell us](#) how this access benefits you. Your story matters.



Combinatorial screening of 3D biomaterial properties that promote myofibrogenesis for mesenchymal stromal cell-based heart valve tissue engineering

Jenna Usprech^{a, c}, David A. Romero^b, Cristina H. Amon^{a, b} and Craig A. Simmons^{a, b, c*}

^a Institute of Biomaterials and Biomedical Engineering, University of Toronto, 164 College Street, Toronto, Ontario M5S 3G9, Canada

^b Department of Mechanical and Industrial Engineering, University of Toronto, 5 King's College Road, Toronto, Ontario, M5S 3G8, Canada

^c Translational Biology and Engineering Program, Ted Rogers Centre for Heart Research, 661 University Ave, Toronto, Ontario, M5G 1M1, Canada

* Correspondence to:

Craig A. Simmons

Translational Biology and Engineering Program, Ted Rogers Centre for Heart Research

University of Toronto

661 University Ave, 14th floor

Toronto, ON, M5G 1M1

c.simmons@utoronto.ca

Telephone: 416-978-8660

Fax: 647-478-5836

1.0 INTRODUCTION

Heart valve replacement is needed when maladaptive matrix remodelling in diseased or congenitally defective heart valves causes them to either fail to support the mechanical loads that they have evolved to endure, or become excessively stiff and cease to exhibit sufficient compliance for normal function. Heart valve tissue engineering attempts to address these failures by replacing dysfunctional tissues with cell-laden structures that provide immediate and appropriate mechanical support, while possessing the capacity for growth and repair.

In native heart valves, growth during development and repair postnatally involves the activation of fibroblasts within the valve interstitium to myofibroblasts [1]. Valve myofibroblasts, identified by their expression of α -smooth muscle actin (α -SMA) [2], are synthetic cells that secrete and assemble collagen and other extracellular matrix proteins [3]. When unchecked, valve myofibroblasts can cause fibrosis leading to valve dysfunction [4, 5], but normal physiological growth and repair processes require regulated matrix synthesis by myofibroblasts. Similarly, myofibroblasts are responsible for matrix synthesis and maturation in valve tissue engineered *in vitro* [1] to achieve the native valve-like mechanical properties required for immediate function upon implantation [6, 7]. Thus, regeneration of heart valve tissues requires strategies to predictively promote myofibroblast generation and synthetic function from viable cell sources.

Human mesenchymal stromal cells (MSCs) are a promising cell source for heart valve tissue engineering due to their multi-potency towards relevant lineages, their abundance in the human body, and their immunoprivileged status [8]. Additionally, a small proportion of MSC-like progenitors exist within the population of valvular interstitial cells that occupy mature heart valve tissue [10]. The generation of connective tissues *in vitro* through the expansion, culture and conditioning of MSCs encapsulated into 3D scaffolds has been implemented with some clinical success for bone [11] and skin applications [12], but has yet to be achieved for heart valves. It is probable that traditional *in vitro* culture conditions have yielded suboptimal tissues, unfit for the clinic, due to a failure to consider the integrative cellular microenvironment. A myriad of interacting environmental factors have been implicated in the differentiation of MSCs, including chemical, mechanical and structural cues [13-15]. Such factors have been studied extensively *in vitro* in isolation but, except for a couple of notable exceptions [16, 17], have not been studied in

combination or when cells were encapsulated in 3D. This is despite mounting evidence suggesting that the integration of these factors is essential for determining cell fate and function [18]. Combinatorial studies are enabled by microarray platforms, such as those developed by Dolatshahi-Pirouz et al., who reported a 3D microarray that was used to encapsulate hMSCs in gelatin methacrylate hydrogels for the purpose of combinatorially assessing osteogenesis for tissue engineering applications [17]. The differentiation of valvular interstitial cells to myofibroblasts in relation to biomaterial and bound biochemical cues was recently investigated in a combinatorial manner [19], however, understanding how the differentiation of MSCs to myofibroblasts occurs for heart valve tissue engineering has not been assessed. Other recent advances in 3D microarray technologies provide additional support towards investigating the synergism of multiple cues in directing cell fate for understanding disease processes or for tissue engineering [16, 20, 21].

Systematic investigation of microenvironmental control of MSCs is aided by the use of engineered materials [14], like synthetic hydrogels, and the design and interpretation of large factorial data sets by statistical techniques. Synthetic hydrogels, like polyethylene glycol norbornene (PEG-NB), largely decouple prescription of mechanics and chemistry, such that, for example, the elastic moduli can be varied while maintaining a constant concentration of ECM-inspired cell adhesive sites [22, 23]. When combined with multi-factorial experimental design and analyses – moving away from one factor at a time (OFAT) approaches [24] – non-intuitive interactions can be revealed. In particular, in select recent studies, statistical analyses with response surface methodology have facilitated the prediction of ideal combinations of parameters for stem cell differentiation and hydrogel composition [20, 25-28].

Here, we developed a platform and analytical workflow that broadly enables systematic screening of multiple environmental factors for their role in influencing cell responses. We report using the platform to screen biomaterial and biochemical factors that promote a myofibroblastic cell phenotype, characterized by enhanced α -SMA and collagen type I expression, from MSCs. Our results illustrate the complex interplay between multiple environmental cues in regulating MSC differentiation, and support the need for combinatorial experimental design and modeling to design biomaterials for predictive control of cell responses.

2.0 MATERIALS AND METHODS

2.1 Poly (ethylene glycol) (PEG) functionalization with norbornene

Norbornene-functionalized PEG (PEG-NB) was synthesized as described previously [23, 29, 30]. Briefly, solid 8-arm PEG-OH (tripentaerythritol core, 20 kDa MW, JenKem USA), 4-(dimethylamino) pyridine (DMAP, Sigma-Aldrich) and pyridine (Sigma-Aldrich) were dissolved in anhydrous dichloromethane (DCM, Fluka). In a separate round-bottom flask, N, N'-dicyclohexylcarbodiimide (DCC, Fluka) and 5-norbornene-2-carboxylic acid (Sigma-Aldrich) were dissolved in anhydrous DCM. Norbornene carboxylic acid was covalently coupled to the PEG-OH at the carboxyl group by adding the contents of the PEG flask dropwise to the norbornene vessel under stirred, anhydrous conditions overnight. Urea was removed from the reaction mixture using a glass fritted funnel and the filtrate was precipitated in ice cold ether (Fisher). The precipitated PEG-NB was collected from a Buchner funnel and dried overnight. To remove excess norbornene carboxylic acid, PEG-NB was dissolved in deionized H₂O, dialyzed in deionized H₂O for at least 3 days, and filtered through a 0.45 µm pore-size syringe filter. The aqueous PEG-NB solution was snap frozen using liquid nitrogen and subsequently lyophilized. Functionalization of PEG with norbornene groups was quantified using proton nuclear magnetic resonance spectroscopy (NMR)(Department of Chemistry, University of Toronto). The percent functionalization of norbornene groups onto PEG-OH arms was 99%, determined by utilizing the norbornene-associated alkene groups located at 5.8-6.2 PPM [29].

2.2 Characterization of acellular PEG-NB hydrogel properties

Compressive moduli, gel fractions, swelling ratios, and mesh sizes were determined for acellular, cell degradable 5 - 11 w/v % PEG-NB hydrogels. Hydrogels were polymerized using an Omnicure S2000 UV light source (Lumen Dynamics) at 7.6 mW/cm² for 60 s in the bore of a 1 mL syringe, resulting in final gel dimensions of roughly 5 mm diameter and 1.8 mm thickness. Hydrogels contained 5, 8, or 11 w/v % (2.5, 3.25 or 4 mM) PEG-NB, a 35% crosslinking density (5.6 mM MMP-degradable peptide sequence CKCGGPQGIWGQGCKC), 6 mM CGRDGS, and 0.05% w/v Irgacure 2959 photoinitiator (BASF) in deionized water. All peptides were custom ordered from Genscript and all experiments contained six replicates per condition. Hydrogels were tested in unconfined compression using a commercial mechanical testing system (Test

Resources 840 series) with 25 g load cell (Honeywell). Images of the hydrogels were taken from above for cross sectional area measurements and from the side for thickness measurements using ImageJ (NIH) before testing. Each sample was compressed to 20% strain for a total of 5 cycles at a strain rate of 10% per minute. The compressive modulus was calculated from the stress-strain curve of the 5th cycle in each test between 10 and 20% strain [31]. Determination of gel fractions and mass swelling ratios were performed according to protocols outlined by Lin et al [32]. For gel fraction tests, which can signify efficiency in crosslinking, the hydrogels were immediately lyophilized after polymerization. After lyophilization to remove all water, hydrogels were weighed (weight 1) and placed in deionized water for 24 hr to dissolve all unreacted monomer. Hydrogels were then lyophilized and weighed again (weight 2). The fraction of weight 2 divided by weight 1 reflects the solid gel fraction that remains after residual unreacted monomer is removed from the hydrogel. The swelling properties of PEG-NB hydrogels can be used to determine constraints on culture vessel dimensions and enable calculation of mesh size, which refers to the distance between consecutive crosslinks in a hydrogel and is indicative of porosity and diffusivity [32]. In a similar process, the gravimetric swelling ratio was determined by placing gels in deionized water for 24 hr immediately after polymerization followed by lyophilization. After lyophilization, the gels were weighed (weight 1). Gels were then placed in 1 x PBS for 48 hrs to promote swelling, after which they were weighed again (weight 2). The fraction of weight 2 divided by weight 1 corresponded to the swelling ratio. The mesh size of hydrogels was calculated using Flory Rehner theory from the gravimetric swelling ratio [32, 33].

2.3 Human mesenchymal stromal cell culture

Human bone-marrow derived mesenchymal stromal cells (hMSCs) were obtained from the Texas A&M Health Science Center College of Medicine Institute for Regenerative Medicine at Scott & White through a grant from ORIP of the NIH, Grant # P40OD011050 (donor #8001R), and were expanded to passage 4. hMSC potential towards osteogenic and adipogenic lineages was confirmed in addition to establishing a colony forming unit frequency greater than 30%. Cells at passage 4 were used for all experiments. Expansion and maintenance of hMSCs occurred in complete culture media, which contained α -MEM supplemented with 2-4 mM L-glutamine, 16.7% fetal bovine serum, and 1% penicillin/streptomycin.

2.4 Polymerization of cell-laden PEG-NB arrays

The adhesion peptides RGD, YIGSR, and DGEA were incorporated into PEG-NB gels that were crosslinked using the MMP-degradable peptide sequence. Scrambled peptide sequences including RDG, GYSRI, and EGEA were also incorporated into the gels in order to maintain a constant peptide loading of 6 mM per hydrogel solution. To encapsulate cells, the harvested cells were re-suspended in α -MEM (without FBS) and subsequently mixed 1:1 with PEG-NB solution, which contained a final concentration of 5 - 11 w/v % (2.5 - 4 mM) PEG-NB, a 35% crosslinking density (5.6 mM CKCGGPQGIWGQGCKC), 0 - 2 mM of CGRGDS, CGRDGS, CDPGYIGSR, CDPGGYSRI, CDDGEA, and CDEGEA, 0.05% w/v Irgacure 2959 photoinitiator, and 1×10^6 cells/mL. In order to create PEG-NB hydrogel arrays, stencils were laser cut (using a VLS3.5 Laser Platform from Universal Laser Systems) out of PDMS to yield squares containing 16 cylindrical holes measuring 2 mm in diameter, 500 μ m height, and spaced 3.5 mm apart. A silicone “window” was placed on top of the stencil to border the 16-hole array. In order to create the arrays, different cell-laden PEG-NB hydrogel formulations were pipetted (2 μ L) into separate holes of the stencil and cured by UV at 7.6 mW/cm² for 60 s. After initial curing, 8 w/v % PEG-NB, crosslinked with the non-cell-degradable PEG dithiol (3.4 kDa, Laysan Bio), was pipetted on top of the array inside the PDMS window and subsequently cured under UV light for 60 s. The two-stage curing process, first implemented by Nguyen et al., allows for covalent bonding to occur between free thiol groups on the cell-laden hydrogel posts and norbornene groups on the non-cell-degradable PEG-NB base [23]. The cell laden hydrogel arrays were cultured in complete culture media with and without 5 ng/mL recombinant human TGF- β 1 (Peprotech), to stimulate myofibrogenesis, and were maintained in a humidified 37 °C incubator with 5% CO₂. Media changes and TGF- β 1 supplementation occurred every two days.

2.5 Immunostaining of α -smooth muscle actin, collagen type I and Hoechst

hMSCs encapsulated in the PEG-NB hydrogels were co-stained with mouse monoclonal anti- α -smooth muscle actin (α -SMA) (F3777, Sigma) and rabbit monoclonal anti-collagen type I (ab138492, Abcam) antibodies, and Hoechst 33342 (P162249, Fisher) after 7 days of culture. To fix the PEG-NB gel arrays, arrays were thrice washed with 1 x PBS followed by incubation with 10% neutral buffered formalin fixative for 30 minutes at room temperature (RT). Arrays were subsequently washed with 1 x PBS and stored at 4 °C prior to staining. To prepare fixed samples

for immunostaining, gel arrays were first washed with 1 x TBS buffer containing 0.1% Triton X-100 (TBST-0.1%) and subsequently permeabilized with TBS containing 0.25% Triton X-100. Arrays were then blocked with 10% bovine serum albumin in TBS for 1 hr at RT. After blocking, arrays were incubated with rabbit anti-collagen type I primary antibody (1:600) in TBS containing 5% goat serum (GS) overnight at 4°C. The next day, arrays were washed with TBST-0.1% four times and subsequently blocked with 10% goat serum in TBS for 1 hr at RT. After blocking, gels were incubated in the dark with Alexa Fluor 568 goat anti-rabbit secondary antibody (1:300) in TBS containing 5% GS for 1.5 hr at RT. Gels were then washed four times with TBST-0.1% and incubated with mouse anti- α -SMA conjugated to FITC (1:300) in TBS with 5% GS for 1.5 hr at RT. Next, arrays were washed four times with TBST-0.1% and incubated with Hoechst (1:1000) for 15 minutes. Arrays were washed again, first with TBST-0.1%, then with deionized water. Finally, 1.5 mL Fluoromount and 0.5 mL deionized water was added to each array for signal preservation prior to imaging with confocal microscopy.

2.6 Confocal microscopy imaging and analysis

A Nikon A1R-A1 laser scanning confocal microscope with 10x objective (CFI Plan Apo λ 10x /0.45, Nikon) was used to image optical slices (z stacks) throughout the entire volume of our 3D constructs. The 3D rendering and analysis software, Imaris (Bitplane), was utilized to create automatically thresholded, quantifiable 3D surfaces around stained objects in the hydrogels. To assess myofibroblastic differentiation, the average α -SMA intensity of cells in a given condition was normalized to the average intensity across all conditions in an experiment. This was to allow normalization of bulk intensity differences that could be attributed to different days of staining and analysis. For collagen type I expression, the total volume of collagen stained surfaces was normalized to the total volume of all nuclear surfaces in a given condition as collagen could be found both intra- and extracellularly.

2.7 Statistical analysis and design of experiments

Statistical analyses were performed using JMP 11 (SAS Institute). Characterization data for the acellular PEG-NB gels are reported as mean \pm standard error of the mean (SEM) and were analyzed by one-way ANOVA with Tukey's post-hoc test for pairwise comparisons. Face-centered central composite designs (CCDs) were randomized and repeated four times. A CCD

was chosen because of its efficiency in detecting two-factor interactions and quadratic effects with the utilization of less resources than full factorial designs [24, 34]. Parametric and non-parametric models were created on the pooled data.

2.8 Parametric models

In a process reported previously [24], response surfaces could be modeled by linear regression using JMP. For example, for a two factor response surface, the output response (Y) could be modelled as a function of independent inputs (x_i) in a polynomial function Eq. (1),

$$Y = K + \beta_1 x_1 + \beta_2 x_2 + \beta_{12} x_1 x_2 + \beta_{11} x_1^2 + \beta_{22} x_2^2$$
 where K corresponds to the average response of centre points, β_i the main effect coefficients, β_{ij} second-order interaction coefficients and β_{jj} quadratic coefficients. The design matrix and coded values are shown in Supplemental Data, Table S1, which represent a four factor screening experiment, replicated with or without TGF- β 1. Coded values were useful in our analysis as they allow the determination of factor effects independent of units through the comparison of β coefficients [34]. Model parameters were estimated using least squares estimation in JMP and the statistical significance of each parameter was evaluated with $p < 0.05$. Through an iterative process of backward elimination [24], insignificant factors ($p > 0.05$) were removed from the initial model and model parameters were calculated from the reduced model. The logarithm of normalized α -SMA intensity and morphology, and the cubed root of normalized collagen type I volume were taken to ensure a normal distribution of the data with equal variance for all data sets.

2.9 Non-parametric models

Non-parametric regression models were created as described previously [27]. The non-parametric models were based on Gaussian random functions [35, 36] which make no explicit assumptions about the functional form of the relationship between dependent and independent variables [37]; only the smoothness of the function is assumed by selecting a kernel function to build the regression model [38].

3.0 RESULTS

3.1 Characterizing PEG-NB hydrogel properties and generating a 3D screening platform

The compressive bulk modulus was determined for PEG-NB hydrogels ranging from 5 – 11 wt% and a range of ~ 5 - 22 kPa was demonstrated (Figure 1A). Gel fraction experiments demonstrated that all gels retained at least 90% of their initial dry weight and did not significantly differ from one another (Figure 1B). However, there was a significant decrease observed in swelling ratio and mesh size between 5 wt% and the 8 and 11 wt% PEG-NB gels, suggesting that a higher monomer composition contributed to a less swollen hydrogel network with smaller pores (Figure 1C and D).

Hydrogel arrays with various formulations of PEG-NB wt% and cell adhesion peptides were generated in custom stencils (Figure 1E and F).

3.2 Screening biomaterial and chemical factors in static cultures to direct myofibroblastic differentiation

Permutations of RGD, DGEA, and YIGSR at different concentrations (0 - 2 mM) were incorporated into 5 - 11 wt% PEG-NB hydrogels containing hMSCs, which were cultured for 7 days with 0 or 5 ng/mL TGF- β 1. α -SMA expression, α -SMA positive cell morphology (sphericity), and collagen type I expression, analyzed using the 3D software Imaris (Figure 2A), were modeled using least squares estimation and both parametric regression and non-parametric regression techniques. Prediction expressions for the reduced parametric models are shown in Supplemental Data, Table S2.

3.2.1 α -SMA expression:

Parametric regression analyses revealed that in the presence of TGF- β 1, PEG-NB hydrogel wt% was the most significant factor influencing myofibroblast differentiation, with greater α -SMA staining intensity manifesting at lower gel wt% (Figure 2B). With TGF- β 1, RGD concentration had a positive biphasic effect on α -SMA staining intensity indicated by the significant main and quadratic RGD parameter estimates (Figure 2B). For the most part, a higher concentration of RGD resulted in higher α -SMA intensities, with an optimal concentration of RGD predicted to 1.9 mM based on the developed model (using the optimization algorithm, Solver, in Excel).

RGD concentration also interacted significantly with PEG-NB wt% (Figure 3) in that higher α -SMA intensities depended on both a low PEG-NB wt% and high RGD concentration (Figure 4). Non-parametric models were consistent, with RGD and PEG-NB wt% having the most sizeable effects on α -SMA intensity (Supplemental Data, Figure S1).

While hMSCs expressed α -SMA in the absence of exogenous TGF- β 1, there were no significant differences in α -SMA intensity to allow for modeling by parametric regression, suggesting that α -SMA expression is only significantly sensitive to material properties in the presence of TGF- β 1. In general, α -SMA staining intensity was enhanced with TGF- β 1 as evidenced when comparing identical gel conditions within an experiment that have been supplemented with 5 ng/mL or 0 ng/mL TGF- β 1 (Figure 3C and D).

3.2.2 Cell morphology:

The cell shape (sphericity) of α -SMA stained cells could be modeled by the same parameters as α -SMA expression, but with different parameter estimate magnitudes (Figure 2). Regardless of TGF- β 1 addition, the negative biphasic effect of RGD concentration had the most significant impact on cell shape, although the magnitude of this non-linear effect was more pronounced with TGF- β 1 (Figure 2C). Cells spread out maximally (sphericity value closer to 0) at RGD concentrations of 1.63 mM and 1.67 mM RGD with and without TGF- β 1, respectively. The effect of PEG-NB wt% on cell shape was positive, indicated by the increased sphericity of cells as wt% increased, irrespective of TGF- β 1 supplementation (Figure 2C). The interaction of RGD concentration and PEG-NB wt% was also significant (Figure 2C), such that higher concentrations of RGD and low levels of PEG-NB wt% led to a more spread cell shape (Figure 4). Although the response surface patterns are similar, TGF- β 1 seemed to incite cell spreading across a larger range of PEG-NB wt% and RGD concentrations (Figure 4A and B). Like with α -SMA intensity, non-parametric modeling corresponded with the parametric model patterns in which RGD and PEG-NB wt% had the most sizeable impact on cell shape regardless of TGF- β 1 supplementation (Supplemental Data, Figure S2).

3.2.3 Collagen type I expression:

As was the case for α -SMA expression and cell shape, collagen type I expression (volume of collagen staining) with or without TGF- β 1, was strongly dictated by PEG-NB wt% (Figure 2D).

Without TGF- β 1, PEG-NB wt% had a negative, slightly biphasic effect on collagen expression, suggesting that as PEG-NB wt% decreases, collagen expression approaches a maximum (Figure 5A). For collagen expression, RGD did not interact with PEG-NB wt% as was evident from the parameter estimates and response surface, however, RGD and DGEA did interact to a small degree (in comparison to the effect of PEG-NB wt%) in the absence of TGF- β 1 (Supplemental data, Figure S3). Non-parametric results display the same main trends that the parametric regression showed in that PEG-NB wt% was the most dominant significant parameter (Supplemental Data, Figure S4). However, non-parametric statistics additionally revealed that when PEG-NB wt% is held constant at 5 wt%, the greatest collagen deposition was evident at a maximal concentration of YIGSR and medial concentrations of RGD and DGEA (Figure 5E).

Similar to conditions that were not supplemented with TGF- β 1, parametric modeling demonstrated that collagen expression of TGF- β 1 supplemented cultures was also strongly enhanced with decreasing PEG-NB wt% (Figure 2). Again, the PEG-NB wt% effect was biphasic, however, in this instance collagen expression increased as PEG-NB wt% decreased without visibly reaching a plateau (Figure 5B). RGD concentration had a small, but significant positive effect on collagen expression and there were no discernable significant peptide interactions (Figure 2). These patterns were echoed in the non-parametric analyses in that low PEG-NB wt% clearly enhanced collagen deposition (Supplemental Data, Figure S4). For TGF- β 1 supplemented cultures, non-parametric models also show an optimal set of peptide concentrations for maximal collagen deposition, but they differ considerably from those identified without TGF- β 1 supplementation. Namely, collagen deposition was the greatest when culture conditions had medial concentrations of YIGSR, mid-high concentrations of DGEA, and a maximal concentration of RGD (Figure 5F).

Although spatial differences in collagen deposition were not investigated directly in this paper, it was observed that in most conditions which demonstrated collagen expression, collagen deposition occurred preferentially within the top 100-200 μ m of the gel arrays (Figure 5D).

4.0 DISCUSSION

MSC fate is determined by multiple interacting micro-environmental cues. In order to screen for combinations of cues that would maximally drive hMSC myofibrogenesis *in vitro*, we developed a hydrogel array platform to systematically test the combinatorial effects of biomaterial and biochemical factors on cell shape, α -SMA, and collagen type I expression. Different biomaterial formulations were achieved by changing PEG-NB wt% (to modulate material stiffness), peptide type, and peptide density, and TGF- β 1 was added to culture medium to investigate its interaction with biomaterial formulation on promoting myofibrogenesis. Aside from the dominant effect of low PEG-NB wt% promoting a spread morphology for cells that expressed high levels of α -SMA and collagen, we found that RGD interacted with PEG-NB wt% to enhance α -SMA expression in the presence of TGF- β 1 and cell spreading regardless of whether TGF- β 1 was in the culture medium. Strikingly, non-parametric modelling additionally revealed that the combinations of peptides that maximized collagen expression depended on the presence or absence of TGF- β 1, indicating that biomaterial properties can modulate MSC response to soluble signals.

Polyethylene glycol norbornene (PEG-NB) was chosen as the biomaterial for our array platform because of the ability to control mechanical (stiffness) properties separately from biochemical properties (cell adhesion), while preserving bioactivity of incorporated proteins better than similar materials like PEG-DA [32]. In general, photopolymerizable hydrogels like PEG-NB can support encapsulation of hMSCs with minimal negative implications on viability, in addition to being amenable to patterning into arrays with high fidelity and speed. A variety of peptide sequences have been incorporated into PEG-NB; here, YIGSR (laminin binding domain), DGEA (collagen type I binding motif), and RGD (ubiquitous binding domain present on fibronectin, collagen type I and laminin) were of focus due to their small size and roles in fibroblast and MSC differentiation [39, 40].

PEG-NB wt% played a dominant role in all outputs examined. The weight percentage of PEG-NB pre-polymer was adjusted to obtain hydrogels with mechanical properties that span a compressive modulus range (5 – 22 kPa) known to differentially promote cell differentiation down distinct lineages in 2D [41, 42]. The measured gel fractions indicated efficient crosslinked hydrogel network formation (all gels retained 90% of their initial dry weight and were not significantly different across the range of PEG-NB wt% tested) (Figure 1B). However, as

expected there were significant increases in compressive modulus and decreases in mesh size (between 5 and 8 - 11 wt%) as the weight percent was increased (Figure 1). As a consequence of this inherent link between mesh size and modulus in the range of wt% tested we were unable to decouple the effects of porosity (mesh size) from modulus. Despite the constraints of the gel system, there is some recent evidence, conducted in 2D, that suggest that porosity may not significantly change protein tethering, substrate deformations or the differentiation potential of MSCs [43]. However, the effect of porosity on cell differentiation has not been sufficiently addressed in 3D. Another variable that has been shown to modulate cell fate is degradation-mediated cellular traction [44]. Khetan et al., discovered that MSCs encapsulated in covalently crosslinked hyaluronic acid hydrogels, either permissive or restrictive to degradation (with equivalent elastic moduli), influenced differentiation to osteogenic or adipogenic lineages, respectively [44]. The compressive moduli of the gels utilized by Khetan et al. ranged from 4.3 - 4.5 kPa [44], practically equivalent to our lowest modulus condition at 5 wt% PEG-NB (4.5 kPa, Figure 2). These results challenge data that have previously been reported in 2D in regards to stiffness conditions that promote myofibrogenesis. For culture and conditioning of valvular interstitial cells (VICs) into myofibroblasts, the majority of cells differentiate on gels of at least 25 kPa (5 times the compressive modulus of the 5 wt% PEG-NB gels that were used here [42, 45]). As noted by Chen et al., VICs share many similarities with MSCs and can provide a useful point of comparison for myofibrogenesis [10], particularly since they have been studied extensively with respect to myofibroblast activation. Recently, Mabry et al., cultured VICs in 3D PEG-NB gels in high throughput, and saw comparable patterns of higher SMA expression in lower modulus materials akin to what we observe with MSCs [19]. Analogous to these findings, osteogenic differentiation of MSCs also occurred in softer modulus materials in 3D compared to when they were cultured on 2D substrates [41, 44, 46, 47], which highlight the importance of dimensionality for MSC differentiation. In another paper by Mabry et al., 3D PEG-NB hydrogels led to transcriptional profiles for encapsulated VICs that were more similar to freshly isolated VICs than VICs cultured on 2D PEG-NB hydrogels or on tissue culture polystyrene[48]. As such, experiments performed in 3D lead to conclusions that are likely more physiologically relevant for the heart valve than those drawn from 2D culture. Therefore, the data presented here is suggestive that softer, more readily degradable gels promote myofibrogenesis of hMSCs, which is associated with greater expression of α -SMA and collagen type I.

As observed in our system, TGF- β 1 is known to upregulate α -SMA expression in MSCs [8, 49]. Even though a relationship between TGF- β 1 and enhanced α -SMA expression has been well established, we were able to tease apart the influence of other factors that are also known to contribute to myofibroblast differentiation when all factors are utilized in combination. For example, bound RGD in 3D PEG-NB hydrogels has been shown to influence α -SMA expression, with higher concentrations of RGD (capped at 2mM) increasing the likelihood that the cells will express α -SMA [50]. In line with these previous studies, our experiments demonstrated that higher RGD concentrations positively affected α -SMA expression. As mentioned above, materials that are porous, degradable and exhibit low compressive moduli (low PEG-NB wt%) also correspond to enhanced α -SMA expression. However, our experiments show that these relationships are dependent on the presence of TGF- β 1 as the biomaterial and biochemical factors studied herein do not significantly influence α -SMA expression in its absence.

In experiments that span ranges of material rigidity and cell adhesion, cell shape can be an effective indicator and director of cell differentiation since MSCs are adherent and thrive by interacting and contracting their environment [51]. We were able to determine by both parametric and non-parametric modeling that the sphericity of α -SMA positive hMSCs was dictated by RGD concentration and PEG-NB wt%, but did not depend on TGF- β 1. Although the relationships between RGD concentration and PEG-NB wt% were not identical in the presence or absence of TGF- β 1, they were very similar (Figure 3). Effectively, RGD concentration between 1.63 and 1.67 mM, and 5 wt% PEG-NB gels led to the most spread out cells. Mabry et al., also noticed a larger aspect ratio (more spread morphology) for VICs in 3D PEG-NB gels with higher concentrations of RGD in the absence of TGF- β 1.

Collagen type I expression in our system was primarily dictated by PEG-NB wt% regardless of TGF- β 1 supplementation. However, non-parametric modeling of collagen type I expression at the lowest wt% revealed more nuanced effects of peptides that were dependent on TGF- β 1 supplementation (Figure 5E and F). Without TGF- β 1, medial levels of DGEA and RGD, with YIGSR at higher concentrations showed patterns for enhanced collagen expression. With TGF- β 1, collagen deposition appeared to be the greatest when hydrogels contained medial concentrations of YIGSR, mid-high concentrations of DGEA, and a maximal concentration of RGD; a completely different optimum than when TGF- β 1 was absent. These observations imply

that hMSC response to bound cell adhesion peptides is modulated by soluble TGF- β 1 (or vice versa), a novel observation that highlights the novelty and utility of our approach. Although some of these peptides did not register as significant factors in our parametric analyses, we were able to visualize potential effects non-parametrically since non-parametric models do not constrain a modelled response to a specific shape and therefore, allow for more complex fits.

Gu et al. cultured VICs on PEG-DA substrates and investigated the impact of RGD, DGEA, and YIGSR on markers indicative of calcification and myofibrogenesis [40]. Utilized alone, RGD led to VIC activation, while YIGSR suppressed markers of myofibroblast activation and calcification, and DGEA yielded no differences from control conditions. From our observations, the roles of DGEA and YIGSR appear to be more subtle in our system, but also potentially work in conjunction with one another at certain PEG-NB wt% (for collagen expression in particular). The impact of certain small peptides in combination has been shown previously by Gould et al. to promote greater α -SMA expression than the influence of individual peptides would have had [52]. This lends credence to our combinatorial screening approach as individual peptide effects are assessed alongside peptide interaction effects.

5.0 CONCLUSION

In summary, we present a novel systematic screening platform and methodology to identify how combinations of biomaterial and microenvironmental conditions guide cell phenotypes. The platform involved controlling PEG-NB wt% and adhesion peptides independently and combinatorially in arrays of 3D hydrogels that were supplemented with and without TGF- β 1. Regression modeling was used to dissect correlations between microenvironmental conditions and cell responses. Application of this methodology to probe biomaterial control of hMSC myofibrogenesis revealed that soft hydrogels (low PEG-NB wt%) best promoted spread myofibroblastic cells that expressed high levels of α -smooth muscle actin (α -SMA) and collagen type I, which was in contrast to 2D culture. In conjunction with low PEG-NB wt%, high concentrations of RGD enhanced α -SMA expression in the presence of TGF- β 1 and cell spreading regardless of whether TGF- β 1 was in the culture medium. Importantly, the presence or absence of TGF- β 1 dictated what the optimal combination of peptides were for maximal collagen expression, indicating that biomaterial properties can modulate MSC response to soluble signals. Ultimately, this approach to identify complex relationships between microenvironmental cues and cell responses will enable greater predictive power over stem cell fate in conditions with interacting material design factors.

6.0 ACKNOWLEDGEMENTS

The authors thank Tim Burrow, Oleg Chebotarev, and Dr. William Murphy and lab members Dr. Stefan Zorn, Dr. Eric Nguyen and Dr. Michael Schwartz from the Bioinspired Materials Lab at the University of Wisconsin-Madison for their technical assistance with PEG-NB synthesis. We also acknowledge financial support from a Natural Sciences and Engineering Research Council of Canada (NSERC) discovery grant (RGPIN 327627-06), Canadian Institute of Health Research (CIHR) Operating Grant (MOP-302041), the Canada Research Chair in Mechanobiology to CAS and an NSERC post-graduate doctoral scholarship, NSERC CREATE Program in Microfluidic Applications and Training in Cardiovascular Health (MATCH) scholarship, Ontario Graduate Scholarship, Queen Elizabeth II Graduate Scholarship, and Heart and Stroke Richard Lewar Centre of Excellence (HSRLCE) studentship to JU.

7.0 REFERENCES

- [1] Rabkin-Aikawa E, Farber M, Aikawa M, Schoen FJ. Dynamic and reversible changes of interstitial cell phenotype during remodeling of cardiac valves. *J Heart Valve Dis* 2004;13:841-7.
- [2] Tomasek JJ, Gabbiani G, Hinz B, Chaponnier C, Brown RA. Myofibroblasts and mechano-regulation of connective tissue remodelling. *Nat Rev Mol Cell Biol* 2002;3:349-63.
- [3] Chester AH, Taylor PM. Molecular and functional characteristics of heart-valve interstitial cells. *Phil Trans R Soc Lond Series B, Biol Sci* 2007;362:1437-43.
- [4] Durbin AD, Gotlieb AI. Advances towards understanding heart valve response to injury. *Cardiovasc Pathol* 2002;11:69-77.
- [5] Liu AC, Joag VR, Gotlieb AI. The emerging role of valve interstitial cell phenotypes in regulating heart valve pathobiology. *Am J Pathol* 2007;171:1407-18.
- [6] Robinson PS, Johnson SL, Evans MC, Barocas VH, Tranquillo RT. Functional tissue-engineered valves from cell-remodeled fibrin with commissural alignment of cell-produced collagen. *Tissue Eng Part A* 2008;14:83-95.
- [7] Syedain ZH, Bradee AR, Kren S, Taylor DA, Tranquillo RT. Decellularized tissue-engineered heart valve leaflets with recellularization potential. *Tissue engineering Part A* 2013;19:759-69.
- [8] Kinner B, Zaleskas JM, Spector M. Regulation of smooth muscle actin expression and contraction in adult human mesenchymal stem cells. *Exp Cell Res* 2002;278:72-83.
- [9] Galmiche MC, Koteliansky VE, Briere J, Hervé P, Charbord P. Stromal cells from human long term marrow cultures are mesenchymal cells that differentiate following a vascular smooth muscle differentiation pathway. *Blood* 1993;82:66-76
- [10] Chen JH, Yip CY, Sone ED, Simmons CA. Identification and characterization of aortic valve mesenchymal progenitor cells with robust osteogenic calcification potential. *Am J Pathol* 2009;174:1109-19.
- [11] Liu Y, Lim J, Teoh SH. Review: development of clinically relevant scaffolds for vascularised bone tissue engineering. *Biotechnol Adv* 2013;31:688-705.
- [12] MacNeil S. Progress and opportunities for tissue-engineered skin. *Nature* 2007;445:874-80.
- [13] Das RK, Zouani OF. A review of the effects of the cell environment physicochemical nanoarchitecture on stem cell commitment. *Biomaterials* 2014;35:5278-93.

- [14] Burdick JA, Vunjak-Novakovic G. Engineered microenvironments for controlled stem cell differentiation. *Tissue Eng Part A* 2008;15:205-19.
- [15] MacQueen L, Sun Y, Simmons CA. Mesenchymal stem cell mechanobiology and emerging experimental platforms. *J R Soc Interface* 2013;10:20130179.
- [16] Floren M, Tan W. Three-dimensional, soft neotissue arrays as high throughput platforms for the interrogation of engineered tissue environments. *Biomaterials* 2015;59:39-52.
- [17] Dolatshahi-Pirouz A, Nikkhah M, Gaharwar AK, Hashmi B, Guermani E, Aliabadi H, et al. A combinatorial cell-laden gel microarray for inducing osteogenic differentiation of human mesenchymal stem cells. *Sci Rep* 2014;4:3896.
- [18] Kshitiz, Park J, Kim P, Helen W, Engler AJ, Levchenko A, et al. Control of stem cell fate and function by engineering physical microenvironments. *Integr Biol* 2012;4:1008.
- [19] Mabry KM, Schroeder ME, Payne SZ, Anseth KS. Three-dimensional high-throughput cell encapsulation platform to study changes in cell-matrix interactions. *ACS Appl Mater Interfaces* 2016;8:21914-22.
- [20] Mendes LF, Tam WL, Chai YC, Geris L, Luyten FP, Roberts SJ. Combinatorial analysis of growth factors reveals the contribution of bone morphogenetic proteins to chondrogenic differentiation of human periosteal cells. *Tissue Eng Part C, Methods* 2016;22:473-86.
- [21] Guermani E, Shaki H, Mohanty S, Mehrali M, Arpanaei A, Gaharwar AK, et al. Engineering complex tissue-like microgel arrays for evaluating stem cell differentiation. *Sci Rep* 2016;6:30445.
- [22] Anderson SB, Lin CC, Kuntzler DV, Anseth KS. The performance of human mesenchymal stem cells encapsulated in cell-degradable polymer-peptide hydrogels. *Biomaterials* 2011;32:3564-74.
- [23] Nguyen EH, Zanutelli MR, Schwartz MP, Murphy WL. Differential effects of cell adhesion, modulus and VEGFR-2 inhibition on capillary network formation in synthetic hydrogel arrays. *Biomaterials* 2014;35:2149-61.
- [24] Chen WL, Likhitpanichkul M, Ho A, Simmons CA. Integration of statistical modeling and high-content microscopy to systematically investigate cell-substrate interactions. *Biomaterials* 2010;31:2489-97.

- [25] Jha AK, Tharp KM, Ye J, Santiago-Ortiz JL, Jackson WM, Stahl A, et al. Enhanced survival and engraftment of transplanted stem cells using growth factor sequestering hydrogels. *Biomaterials* 2015;47:1-12.
- [26] Santhanam S, Liang J, Baid R, Ravi N. Investigating thiol-modification on hyaluronan via carbodiimide chemistry using response surface methodology. *J Biomed Mater Res Part A* 2015;103:2300-8.
- [27] Chen WL, Romero DA, Zhong A, Oakes PW, Liu H, Sider KL, et al. Matrix microarray screens reveal Cdc42 as a regulator of matrix-dependent mesenchymal stromal cell osteogenic differentiation *Sci Rep* 2016;Submitted.
- [28] Rehmann MS, Luna JJ, Maverakis E, Kloxin AM. Tuning microenvironment modulus and biochemical composition promotes human mesenchymal stem cell tenogenic differentiation. *J Biomed Mater Res Part A* 2016;104:1162-74.
- [29] Fairbanks BD, Schwartz MP, Halevi AE, Nuttelman CR, Bowman CN, Anseth KS. A versatile synthetic extracellular matrix mimic via thiol-norbornene photopolymerization. *Adv Mater* 2009;21:5005-10.
- [30] Liu H, Usprech J, Sun Y, Simmons CA. A microfabricated platform with hydrogel arrays for 3D mechanical stimulation of cells. *Acta Biomater* 2016;34:113-24.
- [31] Gramlich WM, Kim IL, Burdick JA. Synthesis and orthogonal photopatterning of hyaluronic acid hydrogels with thiol-norbornene chemistry. *Biomaterials* 2013;34:9803-11.
- [32] Lin CC, Raza A, Shih H. PEG hydrogels formed by thiol-ene photo-click chemistry and their effect on the formation and recovery of insulin-secreting cell spheroids. *Biomaterials* 2011;32:9685-95.
- [33] Cruise GM, Scharp DS, Hubbell JA. Characterization of permeability and network structure of interfacially photopolymerized poly(ethylene glycol) diacrylate hydrogels. *Biomaterials* 1998;19:1287 - 94.
- [34] Montgomery DC. *Design and Analysis of Experiments*. 6 ed. New York John Wiley and Sons; 2005.
- [35] Romero DA, Amon CH, Finger S. Multiresponse metamodeling in simulation-based design applications. *J Mech Design* 2012;134:091001-.
- [36] Sacks J, Welch WJ, Mitchell TJ, Wynn HP. Design and analysis of computer experiments. *Statistical Science* 1989:409-23.

- [37] Clark RM. Non-parametric estimation of a smooth regression function. *J R Stat Soc Series B* 1977;39:107-13.
- [38] Altman NS. An introduction to kernel and nearest-neighbor nonparametric regression. *Am Stat* 1992;46:175-85.
- [39] Frith JE, Mills RJ, Hudson JE, Cooper-White JJ. Tailored integrin-extracellular matrix interactions to direct human mesenchymal stem cell differentiation. *Stem Cells Dev* 2012;21:2442-56.
- [40] Gu X, Masters KS. Regulation of valvular interstitial cell calcification by adhesive peptide sequences. *J Biomed Mater Res A* 2010;94:1620-30.
- [41] Engler AJ, Sen S, Sweeney HL, Discher DE. Matrix elasticity directs stem cell lineage specification. *Cell* 2006;126:677-89.
- [42] Chen JH, Chen WL, Sider KL, Yip CY, Simmons CA. Beta-catenin mediates mechanically regulated, transforming growth factor-beta1-induced myofibroblast differentiation of aortic valve interstitial cells. *Arterioscler Thromb Vasc Biol* 2011;31:590-7.
- [43] Wen JH, Vincent LG, Fuhrmann A, Choi YS, Hribar KC, Taylor-Weiner H, et al. Interplay between matrix stiffness and ligand presentation in stem cell differentiation. *Nat Mater* 2014;13:979-87.
- [44] Khetan S, Guvendiren M, Legant WR, Cohen DM, Chen CS, Burdick JA. Degradation-mediated cellular traction directs stem cell fate in covalently crosslinked three-dimensional hydrogels. *Nat Mater* 2013;12:458-65.
- [45] Kloxin AM, Benton JA, Anseth KS. In situ elasticity modulation with dynamic substrates to direct cell phenotype. *Biomaterials* 2010;31:1-8.
- [46] Pek YS, Wan AC, Ying JY. The effect of matrix stiffness on mesenchymal stem cell differentiation in a 3D thixotropic gel. *Biomaterials* 2010;31:385-91.
- [47] Guvendiren M, Burdick JA. Stiffening hydrogels to probe short- and long-term cellular responses to dynamic mechanics. *Nature Commun* 2012;3:792.
- [48] Mabry KM, Payne SZ, Anseth KS. Microarray analyses to quantify advantages of 2D and 3D hydrogel culture systems in maintaining the native valvular interstitial cell phenotype. *Biomaterials* 2016;74:31-41.
- [49] Desai VD, Hsia HC, Schwarzbauer JE. Reversible modulation of myofibroblast differentiation in adipose-derived mesenchymal stem cells. *PLoS One* 2014;9:e86865.

[50] Benton JA, Fairbanks BD, Anseth KS. Characterization of valvular interstitial cell function in three dimensional matrix metalloproteinase degradable PEG hydrogels. *Biomaterials* 2009;30:6593-603.

[51] Kilian KA, Bugarija B, Lahn BT, Mrksich M. Geometric cues for directing the differentiation of mesenchymal stem cells. *Proc Natl Acad Sci USA* 2010;107:4872-7.

[52] Gould ST, Darling NJ, Anseth KS. Small peptide functionalized thiol-ene hydrogels as culture substrates for understanding valvular interstitial cell activation and de novo tissue deposition. *Acta Biomater* 2012;8:3201-9.

8.0 FIGURE LEGENDS

Figure 1: Characterization of PEG-NB gel array properties. A) Compressive moduli, B) gel fraction, D) volumetric swelling ratio and E) mesh size of PEG-NB hydrogels. All experiments had $n = 6$, * $p < 0.05$, ** $p < 0.003$, *** $p < 0.0001$. C) PDMS stencil and silicone window used to generate the hydrogel array platform. F) The array platform consists of cell degradable PEG-NB hydrogel posts covalently bonded to a non-cell degradable PEG-NB base.

Figure 2: A) A representative 3D rendering of a hydrogel where 3D surfaces are created for each laser channel using automatic thresholding in Imaris; surface colours correspond to the immunostaining dyes (α -SMA stained in green, collagen type I in red and Hoechst in blue). A summary of parameter estimates (factor effects) for B) α -SMA intensity, C) hMSC morphology (sphericity), and D) collagen volume. Axis labels correspond to β coefficients in the polynomial function. Larger parameter estimate magnitudes correspond to a larger effect on that particular factor on the model. Error bars denote standard error of the estimated parameters. ** $p < 0.0001$, * $p < 0.05$, # $p < 0.1$.

Figure 3: A) Response surface of the interaction between RGD concentration and PEG-NB wt% on α -SMA intensity average when supplemented with TGF- β 1. Representative maximum intensity z stack projections of gels from one experiment cultured with TGF- β 1 stained with α -SMA in green, collagen type I in red, and Hoechst in blue. Peripheral images are side view projections; B) condition 6 (11 wt% PEG-NB and 0 mM adhesion peptides) and C) condition 4 (5 wt% PEG-NB and 2 mM RGD). D) Condition 4 (5 wt% PEG-NB and 2 mM RGD) cultured without TGF- β 1 is depicted to show the difference in α -SMA staining intensity in cultures that were not supplemented with TGF- β 1.

Figure 4: Response surface of the interaction between RGD concentration and PEG-NB wt% on cell sphericity when supplemented with A) 0 ng/mL or B) 5 ng/mL TGF- β 1. Representative maximum intensity projections of a more rounded cell morphology of α -SMA stained cells is

depicted in C) condition 3 (5 wt% PEG-NB with 2 mM YIGSR) with an average sphericity of 0.85 and an elongated morphology is depicted in D) condition 4 (5 wt% PEG-NB with 2 mM RGD) with an average sphericity of 0.63. Peripheral images are side view projections.

Figure 5: Parametric and non-parametric models for collagen expression. Response surface of the interaction between PEG-NB wt% and RGD on normalized collagen volume, when DGEA is at 0 (1mM), with A) 0 ng/mL and B) 5 ng/mL TGF- β 1. C-D) Representative maximum intensity z stack projections of low and high collagen expressing gels from one experiment stained with α -SMA in green, collagen type I in red, and Hoechst in blue (cultured with 0 ng/mL TGF- β 1, but is also representative for 5 ng/mL TGF- β 1); C) condition 6 (11 wt% PEG-NB and 0 mM adhesion peptides and D) condition 5 (5 wt% PEG-NB and 2 mM RGD, DGEA, and YIGSR). Peripheral images are side view projections. E-F) Non-parametric response surfaces when YIGSR is held constant at 2 mM and cultures are supplemented with E) 0 ng/mL and F) 5 ng/mL TGF- β 1. Scales are condensed to illustrate pattern at higher collagen deposition.

Figure 1
[Click here to download high resolution image](#)

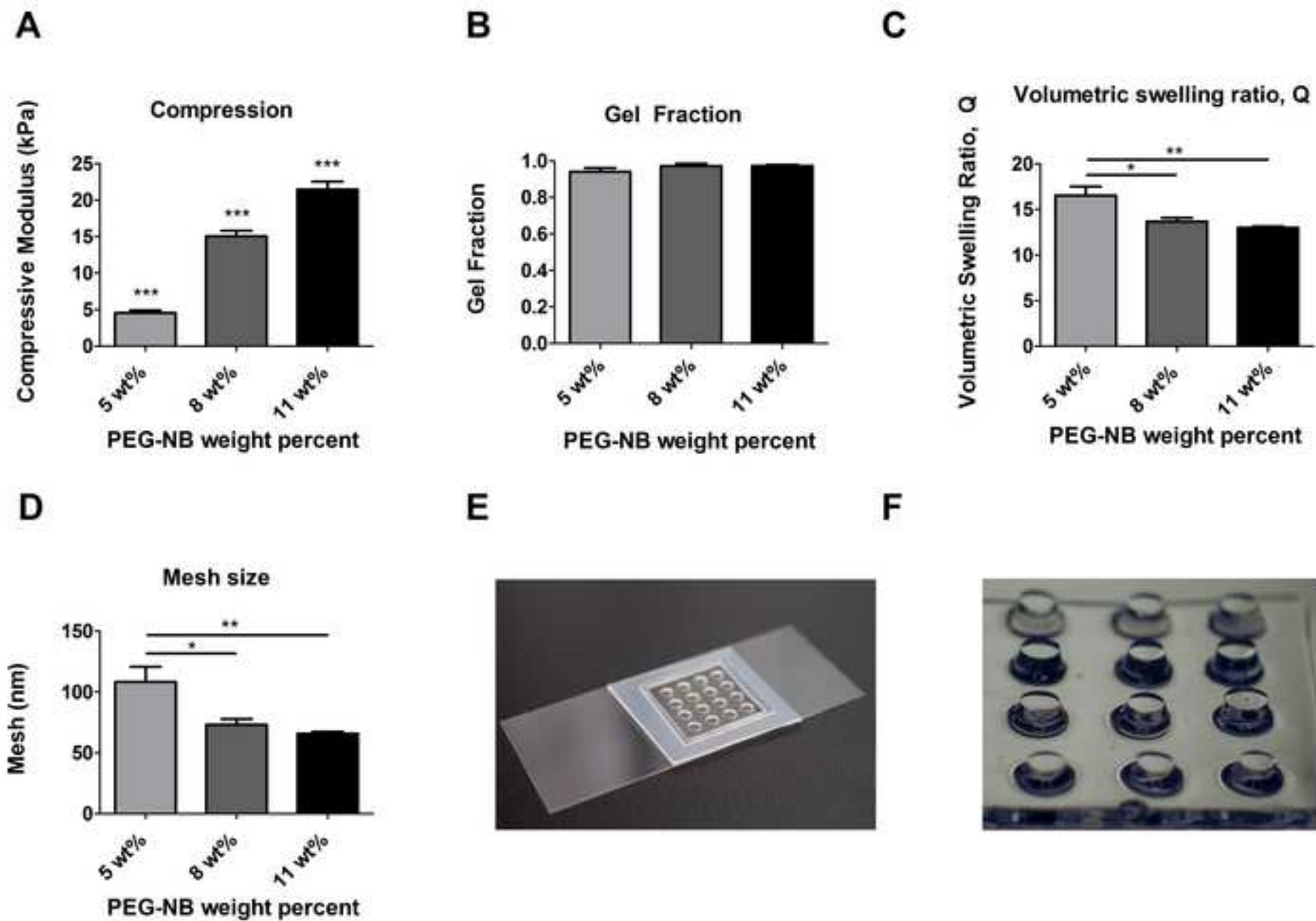


Figure 2
[Click here to download high resolution image](#)

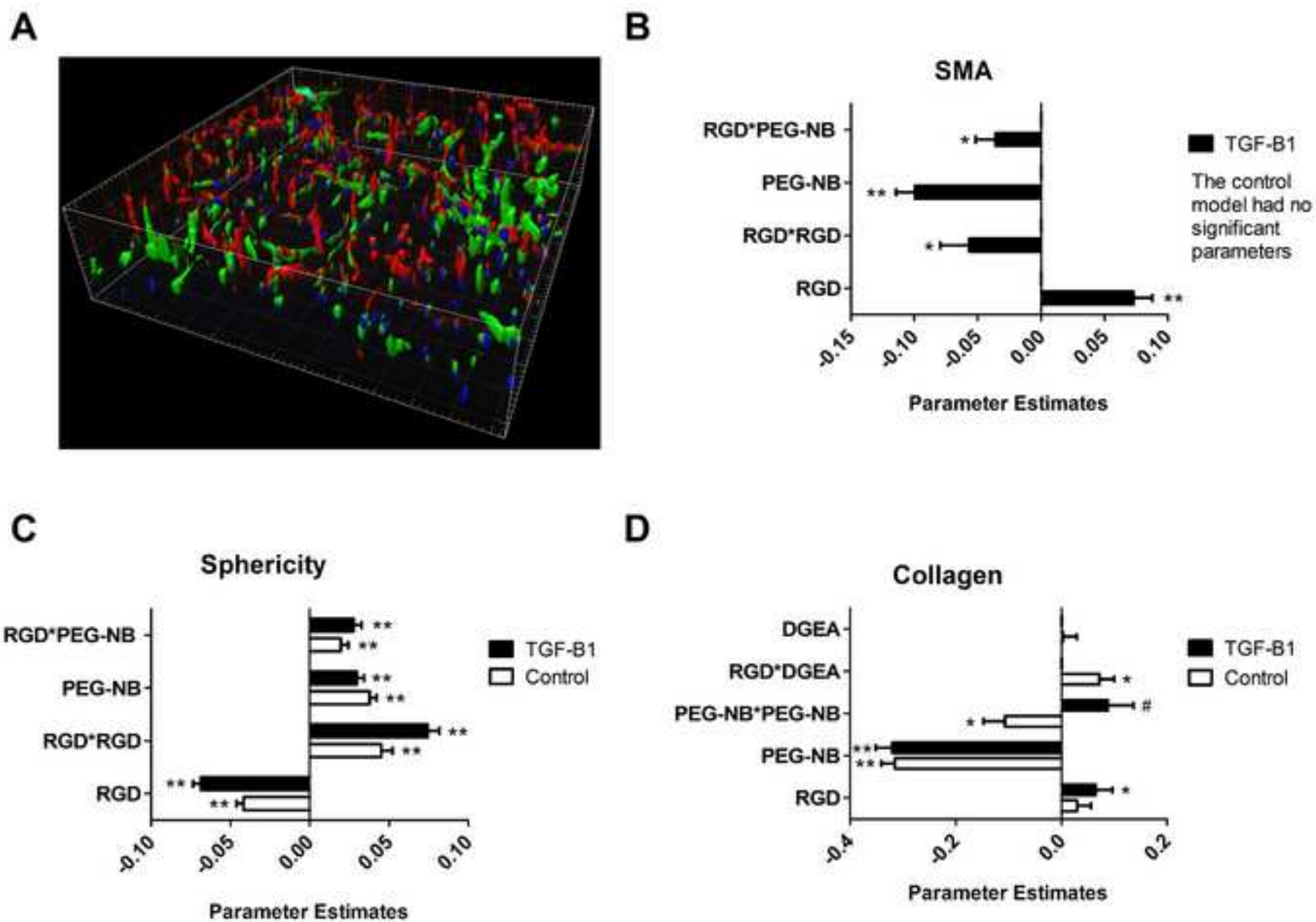


Figure 3
[Click here to download high resolution image](#)

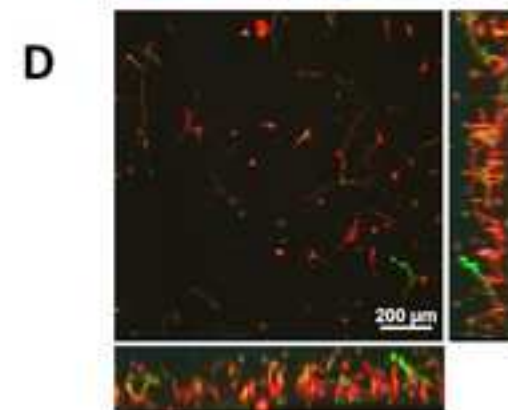
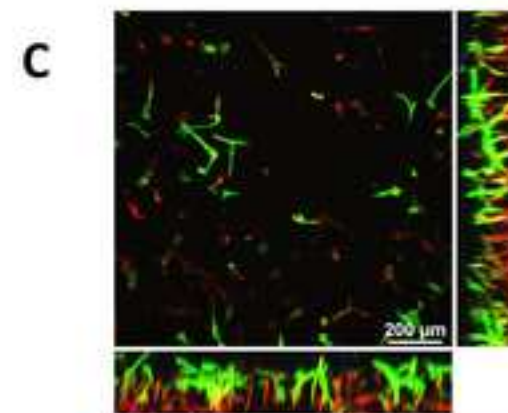
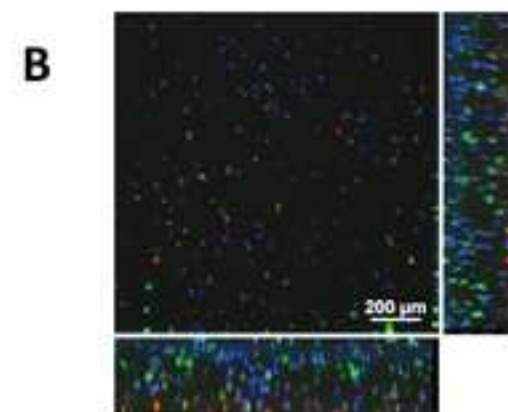
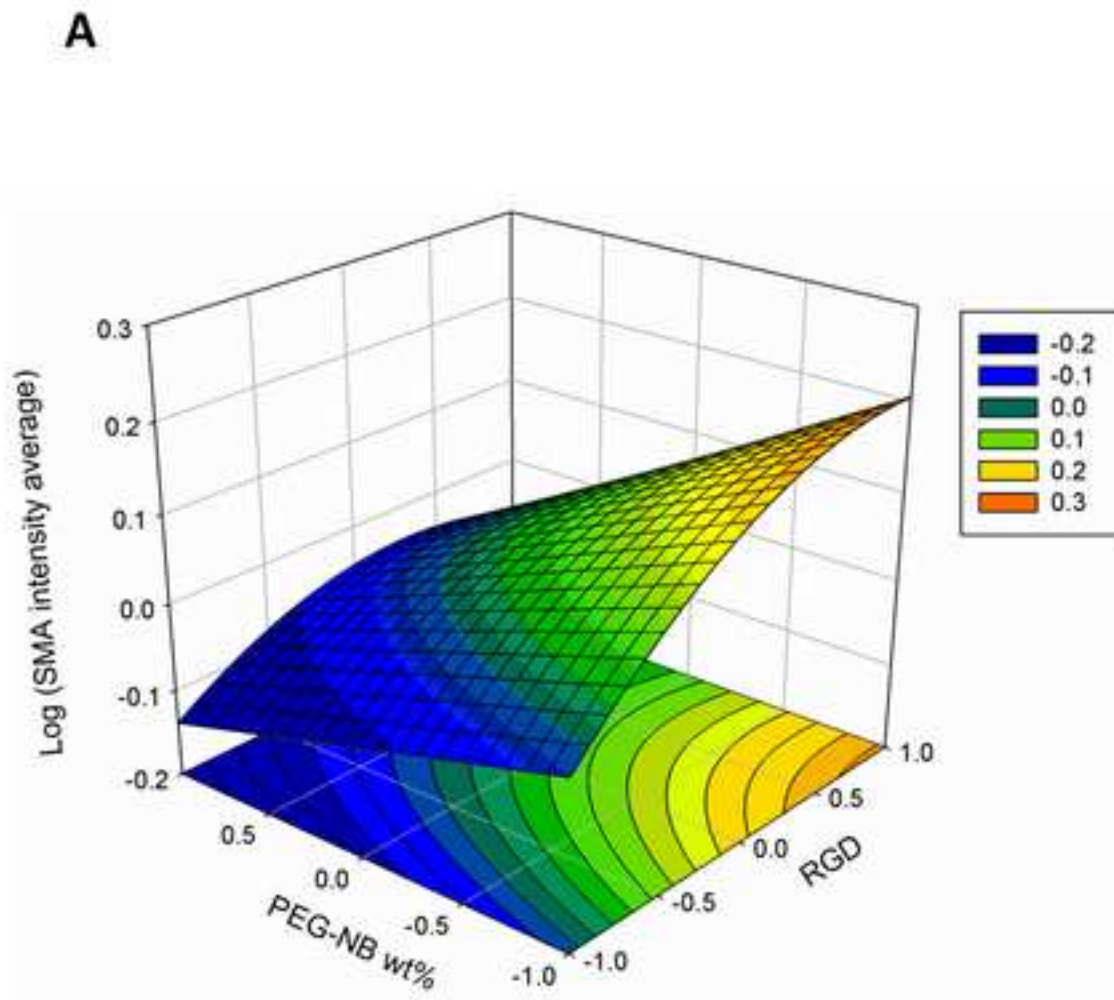


Figure 4
[Click here to download high resolution image](#)

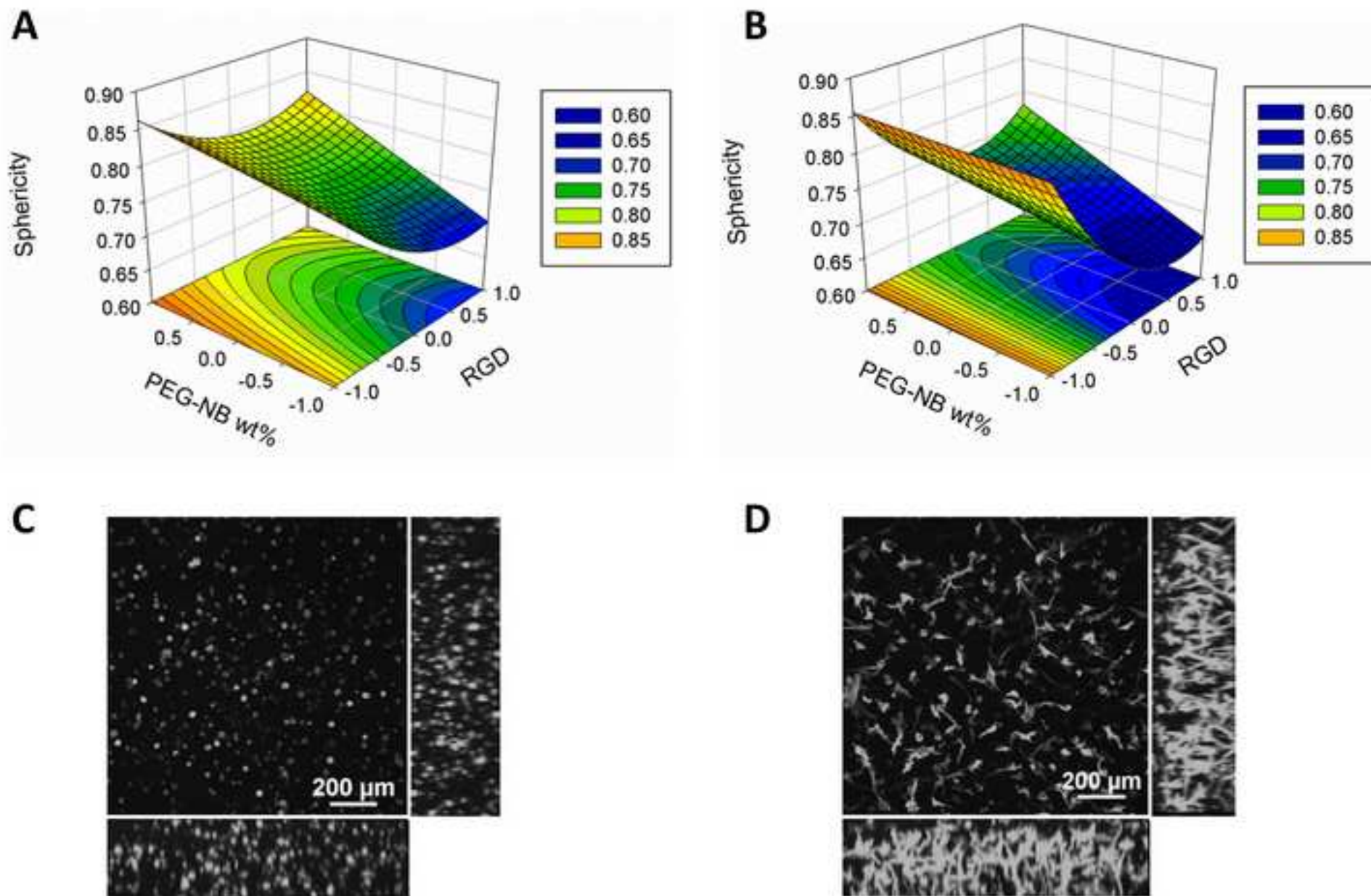
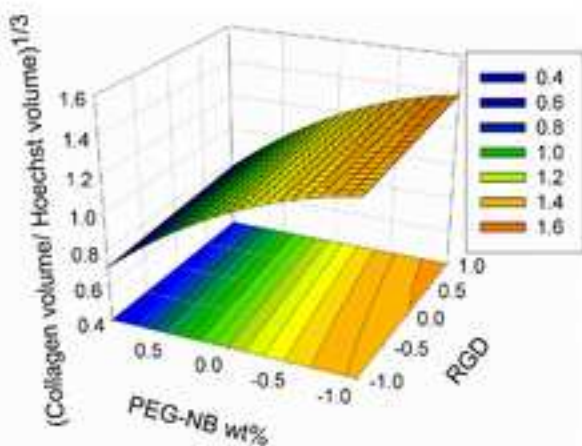
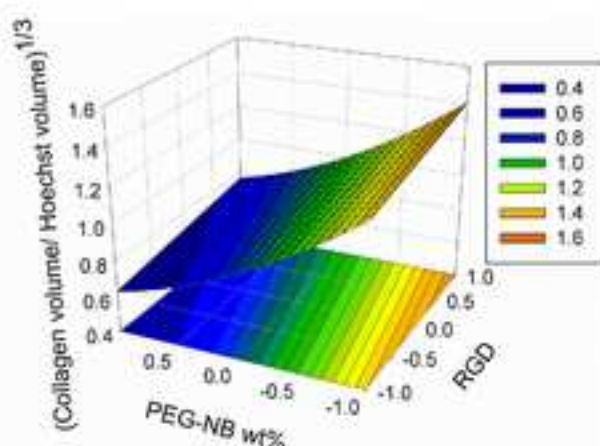


Figure 5
[Click here to download high resolution image](#)

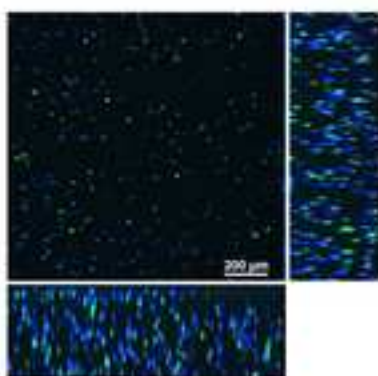
A



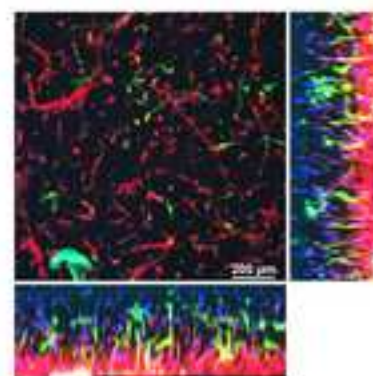
B



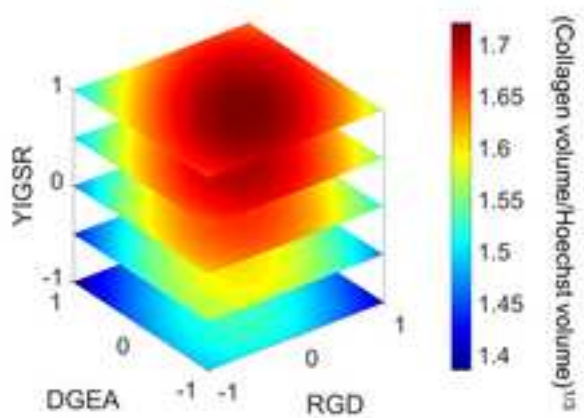
C



D



E



F

